Gyrokinetic Turbulence Simulation Compared with a High Ion Temperature Large Helical Device Experiment

M. Nunami[1], T.-H. Watanabe[1,2], H. Sugama[1,2], and K. Tanaka[1]
[1] *National Institute for Fusion Science, Toki, Gifu 509-5292, Japan*
[2] *The Graduate University for Advanced Studies, Toki, Gifu 509-5292, Japan*
(Dated: October 19, 2011)

Ion temperature gradient turbulent transport in the Large Helical Device (LHD) is investigated by means of gyrokinetic simulations in comparison with the experimental density fluctuation measurements of ion-scale turbulence. The local gyrokinetic Vlasov simulations are carried out incorporating full geometrical effects of the LHD configuration, and reproduce the turbulent transport levels comparable to the experimental results. Reasonable agreements are also found in the poloidal wavenumber spectra of the density fluctuations obtained from the simulation and the experiment. Numerical analysis of the spectra of the turbulent potential fluctuations on the two-dimensional wavenumber space perpendicular to the magnetic field clarifies the spectral transfer into a high radial wavenumber region through the interaction with zonal flows, which correlates with the turbulent transport reduction. The resultant transport levels at different flux surfaces are expressed in terms of a simple linear relation between the transport coefficient and the ratio of the squared turbulent potential fluctuation to the averaged zonal flow amplitude.

Keywords: gyrokinetic simulation, ITG turbulence, zonal flow, anomalous transport, LHD experiment

Helical systems such as stellarators and heliotrons [1] are considered to be one of the promising concepts for the magnetic confinement fusion reactor, because they are advantageous in realizing long-time discharges without external current drives. In addition to the issue of the confinement field optimization for decreasing the neoclassical transport [2], reduction of the anomalous transport, which is caused by the plasma turbulence, is another critical issue for improving confinement properties of helical plasmas [3, 4]. Furthermore, the anomalous transport phenomena make significant roles not only in fusion plasmas but also in more general fields, e.g. astrophysics, space physics and laboratory plasmas [5], as the turbulence is ubiquitously found in the nature. Nowadays, it has been considered that plasma turbulence is determined by the interaction between the microinstabilities such as ion temperature gradient (ITG) modes and zonal flows [6, 7]. To understand the transport physics, we need to study not only ideal and simplified models, but also the concrete experimental results observed in real systems. In recent years, gyrokinetic simulations have been extensively done to investigate turbulent transport processes in tokamaks [8, 9] and helical systems [3, 4, 10, 11]. While there are several publications on validation of the gyrokinetic turbulent transport simulations in tokamaks (for example, Ref. [12]), no direct comparison between gyrokinetic simulations and the experimental data of helical systems has been reported so far. The present study constitutes the first attempt to validate the gyrokinetic simulations of ITG turbulence with the experimental observations in the Large Helical Device (LHD) [13], by elaborately adopting the three-dimensional equilibrium reconstructed from experimental data.

In our previous paper [14], by means of the linear gyrokinetic simulations, we found that the density fluctuations measured by phase contrast imaging (PCI) method in the LHD high ion temperature discharge #88343 [15, 16] have large amplitudes for the radial positions and the poloidal wavenumbers which correspond to ITG modes having large growth rates. In the present work, applying the gyrokinetic Vlasov flux-tube code GKV-X [17], we perform the nonlinear ITG turbulent transport simulations to evaluate the saturation levels of the turbulent fluctuations, zonal flows, and ion heat transport in the LHD discharge #88343. The GKV-X solves the nonlinear gyrokinetic equation for the ion perturbed gyrocenter distribution function, incorporating large number of Fourier components of the confinement field as well as full geometrical information calculated by the three-dimensional MHD equilibrium code VMEC [18]. The quasi-neutrality condition is used and the electron density perturbation δn_e is given in terms of the electrostatic potential ϕ as $\delta n_\mathrm{e}/n_0 = e[\phi - \langle\phi\rangle]/T_\mathrm{e}$, where $\langle\cdots\rangle$ represents the flux surface average and standard notations are used for physical variables. In the GKV-X, the local flux-tube model [19] is used with the field-aligned coordinates $\{x, y, z\}$ which are related with the Boozer coordinates [20] $\{r, \theta, \zeta\}$, as $\{x, y, z\} = \{r - r_0, (r_0/q_0)\,[q(r)\theta - \zeta]\,, \theta\}$ around the flux surface at r_0. Here, $q(r)$ is the safety factor at r, and $q_0 = q(r_0)$. The coordinate $z = \theta$ is defined along the field line labeled by $\alpha = \zeta - q_0\theta =$ constant. The same collision term as in Ref. [10] is employed.

The nonlinear flux-tube ITG turbulence simulations are performed at different radial positions, $\rho = 0.46, 0.65$ and 0.83, independently. Here, ρ is the normalized minor radius defined in Ref. [14]. The experimental results show that $T_\mathrm{i}/T_\mathrm{e} = 1$ is well satisfied for these radial positions, and we assume $n_\mathrm{i}/n_\mathrm{e} = 1$. The simulation

conditions are the same as in previous linear simulations except for the nonlinear term and the collisional effect. The used collision frequency $\nu_{\rm ii} = 0.0025 v_{\rm ti}/R_0$ is so small that its effect on the dispersion relation of the ITG instability is negligible. Here, R_0 is the major radius of the torus. For the ITG turbulence simulation in the helical systems which have complicated magnetic field structures, high resolution along the field line is necessary. Therefore, we used a huge number of the grid points in the five dimensional phase space, $128 \times 128 \times 512 \times 128 \times 64$ in the $(x, y, z, v_\parallel, \mu)$-space. The simulation box size in the velocity space $(v_\parallel, \mu)$ is $-5v_{\rm ti} \le v_\parallel \le 5v_{\rm ti}$ and $0 \le \mu \le 12.5 m_{\rm i} v_{\rm ti}^2/B_0$, where $\mu = m_{\rm i} v_\perp^2/2B_0$ is the magnetic moment . In the real space, we use $-\pi \le z < \pi$ along the field line direction, and the system lengths in perpendicular directions are $L_x = 2\pi/\Delta k_x$ and $L_y = 2\pi/\Delta k_y$, where $(\Delta k_x, \Delta k_y)$ are minimum wavenumbers in (x, y)-space given by $(\Delta k_x \rho_{\rm ti}, \Delta k_y \rho_{\rm ti}) = (0.116,\ 0.035)$, $(0.128,\ 0.038)$, and $(0.122,\ 0.042)$ for $\rho = 0.46, 0.65$, and 0.83, respectively, where $\rho_{\rm ti} \equiv v_{\rm ti}/(eB_0/m_{\rm i}c)$ is the ion thermal gyroradius with the thermal speed $v_{\rm ti} = \sqrt{T_{\rm i}/m_{\rm i}}$.

We have performed comparison of the ion transport level resulting from the simulation with the LHD experimental observation for the first time. In the saturation phase of the turbulence, we evaluate the time-averaged ion heat flux $P_{\rm i}$ defined by integrating the ion heat flux density $Q_{\rm i}$ over the flux surface as $P_{\rm i} = \int Q_{\rm i} dS$ for each radial position. The profiles of the electron density and the ion temperature observed in the LHD experiment #88343 are plotted in Fig.1(a), where the density profile for $\rho < 0.9$ is so flattened that the trapped electron mode, which is not treated in the present model, is considered to be stabilized. Figure 1(b) shows the profile of the ion heat fluxes $P_{\rm i}$ obtained from the GKV-X simulations and from the experiment. The error bars for the simulation results are evaluated from the errors of the ion temperature gradient scale length $L_{T{\rm i}} \equiv -(\mathrm{d} \ln T_{\rm i}/\mathrm{d}r)^{-1}$ obtained from the experimental observation of the ion temperature profile in Fig. 1(a). The simulation results are 15–50 % lower than that in the experimental values which include both the anomalous and neoclassical contributions to the transport. If we subtract the neoclassical part calculated by the GSRAKE code [21], the simulation results agree well with the anomalous part of $P_{\rm i}$, such that the observed differences are less than 10 % for $\rho = 0.46, 0.65$, and about 30 % for $\rho = 0.83$ (see also Table I for the ion heat diffusivity $\chi_{\rm i}$). Figure 2 shows the poloidal wavenumber spectra of the turbulent density fluctuation obtained from the PCI measurement and the simulation, where k_y is treated as the poloidal wavenumber in the coordinates used in the simulation. The both spectra have a peak in a low wavenumber region of $k\rho_{\rm ti} < 0.5$ and similar shape in a high wavenumber region of $k\rho_{\rm ti} > 0.5$, although the peak position of the experimental spectrum is found at a higher wavenumber than that obtained from the simulation. It should be remarked that, because of coarse resolution and the cutoff of the wavenumber at $k_\theta \rho_{\rm ti} \sim 0.2$ in the PCI measurement, the experimental results in lower wavenumber region have a large ambiguity. One of the other possible reasons for the quantitative difference appearing in the lower wavenumber spectra is contributions of kinetic electrons which are not taken into account in the GKV-X code. Nevertheless, the reasonable agreements between the LHD experiments and simulations strongly encourages us to pursue the gyrokinetic simulation studies for the anomalous transport in non-axisymmetric systems.

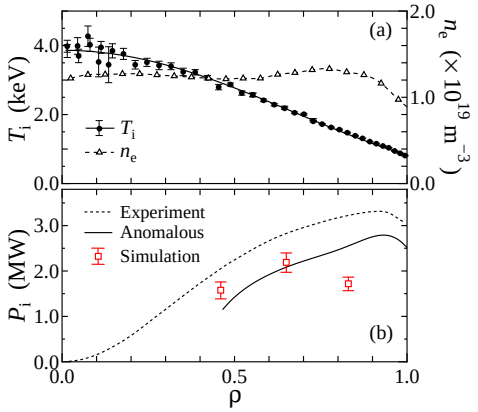

FIG. 1. Radial profiles of (a) the ion temperature $T_{\rm i}$, electron density $n_{\rm e}$ in the LHD experiment #88343, and (b) ion heat flux $P_{\rm i}$ obtained from the experiment (dotted curve) and the GKV-X simulations (open squares with the error bars). The solid curve in (b) represents the anomalous part of the experimental $P_{\rm i}$.

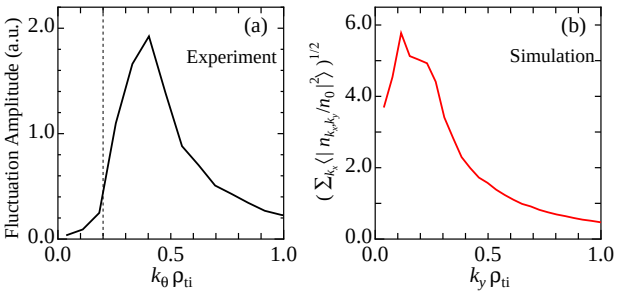

FIG. 2. Poloidal wavenumber spectra for the density fluctuation amplitude obtained from (a) the PCI measurement for $\rho = 0.6$–0.7 in the LHD experiment, and (b) the GKV-X simulations at $\rho = 0.65$. In (a), the dashed line represents the cutoff of the wavenumber in the PCI measurement. The ordinate of (b) is normalized by $R_0/\rho_{\rm ti}$.

It is now widely recognized that the ITG turbulent transport is determined by the competitive interaction between turbulence and zonal flows, and there have been a number of theoretical studies which investigate effects of magnetic geometry on zonal flows in helical systems [22–24]. Figure 3(a) shows the power spectra of the potential fluctuations of the simulations in the k_y space, which are obtained by integrating the potential fluctuations over the k_x space $\sum_{k_x} \langle |\phi_{k_x,k_y}|^2 \rangle / (\Delta k_x \Delta k_y)^{1/2}$, and taking the time average in the saturated phase for

TABLE I. The ion heat diffusivity from the anomalous contribution given by the LHD experiment and from the ITG turbulent transport obtained from the GKV-X simulations in physical unit $\chi_{\rm i}$ [m^2/s], and the gyro-Bohm unit $\chi_{\rm i}^{\rm GB} = \chi_{\rm i}/(\rho_{\rm ti}^2 v_{\rm ti}/R_0)$, where $\rho_{\rm ti} = v_{\rm ti}/(eB_0/m_{\rm i}c)$ and $v_{\rm ti} = \sqrt{T_{\rm i}/m_{\rm i}}$.

	ρ	0.46	0.65	0.83
$\chi_{\rm i}$ [m^2/s]	Experiment	2.40	2.71	2.73
	Simulation	3.60	2.84	1.84
$\chi_{\rm i}^{\rm GB} = \chi_{\rm i}/(\rho_{\rm ti}^2 v_{\rm ti}/R_0)$	Experiment	3.85	6.63	11.59
	Simulation	5.79	6.97	7.80

three simulation runs using different values of ρ. In the plots, we also show the simulation result obtained by using the vacuum (or zero beta) magnetic field configuration at $\rho = 0.65$, where the same simulation parameters of the experiment #88343 at $\rho = 0.65$ are used except for the field configuration. In this vacuum field configuration with no Shafranov shift, the magnetic axis is more inward shifted, the neoclassical transport is lower, and the zonal flow response is better than in the configuration of the experiment as theoretically expected [22]. In the experimental configuration, the spectrum at $\rho = 0.83$ has a peak in a lower region of k_y than those at inner radial positions. The peak amplitude of the fluctuation spectrum at $\rho = 0.83$ in the gyro-Bohm unit, where ϕ_{k_x,k_y} is normalized by $eR_0/T_{\rm i}\rho_{\rm ti}$, is about 5 times higher than that in $\rho = 0.65$ case, and 10 times higher than in $\rho = 0.46$ case. We also find that the peak amplitude in the inward-shifted configuration is larger than in the experimental one. According to the mixing length estimate [25], the turbulent transport is roughly characterized by γ/k_y^2, where γ is the linear growth rate of the mode. For the cases corresponding to those in Fig. 3(a), we plot spectra of γ/k_y^2 in Fig. 3(b), where one finds obvious differences in the low k_y region of $k_y\rho_{\rm ti} < 0.2$–0.3. The peak value of γ/k_y^2 at $\rho = 0.83$ is 5–10 times higher than the other radial positions in the experimental cases. At $\rho = 0.65$, γ/k_y^2 for the the inward-shifted case is higher than that for the experimental case. The peak position shifts to the lower k_y side for the outer radial position in similar to the power spectrum of potential fluctuations in Fig. 3(a). Thus, the turbulence spectra are correlated with the mixing length estimate although it is not simply concluded that mixing length estimate from the linear growth rate solely influences the turbulent transport level, because the interaction between zonal flow and turbulence is also a key ingredient determining the transport. In Fig. 3(d), the two-dimensional spectra in the wavenumber space (k_x, k_y) are shown. Spectra for the experimental case with $\rho = 0.83$ and inward-shifted case clearly spread in the high-k_x region which is caused by the spectral transfer from the low-k_x to the high-k_x space through the interaction between zonal flows and turbulence [26]. The high-k_x modes in the spreading spectrum make less contribution to the transport while they still contribute to the integrated power spectrum shown in Fig. 3(a). Indeed, as shown in Fig. 3(c), larger zonal flows causing the spectrum spreading are generated for $\rho = 0.83$ and inward-shifted cases.

Correlations of the resultant transport level on the turbulence and the zonal flow are examined in the Lissajous plots in Figs. 4 for the squared turbulent potential $T \equiv (1/2)\sum_{k_x,k_y\neq 0}\langle|e\phi_{k_x,k_y}R_0/T_{\rm i}\rho_{\rm ti}|^2\rangle/(\Delta k_x\Delta k_y)^{1/2}$, the averaged zonal flow potential $Z^{1/2} \equiv [(1/2)\sum_{k_x}\langle|e\phi_{k_x,0}R_0/T_{\rm i}\rho_{\rm ti}|^2\rangle/(\Delta k_x\Delta k_y)^{1/2}]^{1/2}$, and the ion heat diffusivity in the gyro-Bohm unit $\chi_{\rm i}^{\rm GB} \equiv \chi_{\rm i}/(\rho_{\rm ti}^2 v_{\rm ti}/R_0)$. In the $Z^{1/2}$-T plot of Fig. 4(a), all plots in the experimental cases seem to be fitted by a simple proportional relation of $Z^{1/2} \propto T$. On the other hand, the result of the inward-shifted case shows the highest ratio of $Z^{1/2}$ to T which implies that the zonal flow components are efficiently generated because of the higher zonal flow response in the inward-shifted or neoclassically optimized configuration [3]. It is seen from the plots in $\chi_{\rm i}^{\rm GB}$-T space of Fig. 4(b) that the transport level is not simply related to the potential fluctuations or the mixing length estimate shown in Figs. 3(a) and (b). On the other hand, one finds in the $\chi_{\rm i}^{\rm GB}$-$(T/Z^{1/2})$ space of Fig. 4(c), that all plots including the inward-shifted case are well represented by the relation $\chi_{\rm i}^{\rm GB} \propto T/Z^{1/2}$, despite the fact that a wide range of conditions for the different radial positions and the inward-shifted case are included here. In fact, more than 95 % of the data points in the saturation phase are confined in the region surrounded by two lines, $\chi_{\rm i}^{\rm GB} = \kappa T/Z^{1/2}$ with $\kappa = (7.2 \pm 2.0) \times 10^{-2}$. We expect that this newly-obtained relation among the ion heat transport, zonal flows, and ITG turbulence in the LHD configurations can be used to construct a formula for the turbulent ion heat diffusivity applicable to the transport code analyses.

In summary, we have presented the first results of direct comparison between the gyrokinetic ITG turbulence simulations and the experimental observations in the high ion temperature LHD plasma. The present GKV-X simulations, which include full geometry data of the LHD configuration, reproduce the turbulent ion heat fluxes obtained from the experiment within errors of about 30%. The ITG turbulence simulations also have shown the poloidal wavenumber spectrum of the density fluctuation which is similar to that of the fluctuation given by the PCI measurement in the LHD except for experimentally ambiguous low wavenumber regions. While we still need to improve the GKV-X code by including other effects such as kinetic electrons and electromagnetic fluctuations, the first validation of the simulation code to the LHD experiment is successful enough to confirm that we are on the right track toward more accurate predictions of the anomalous transport in

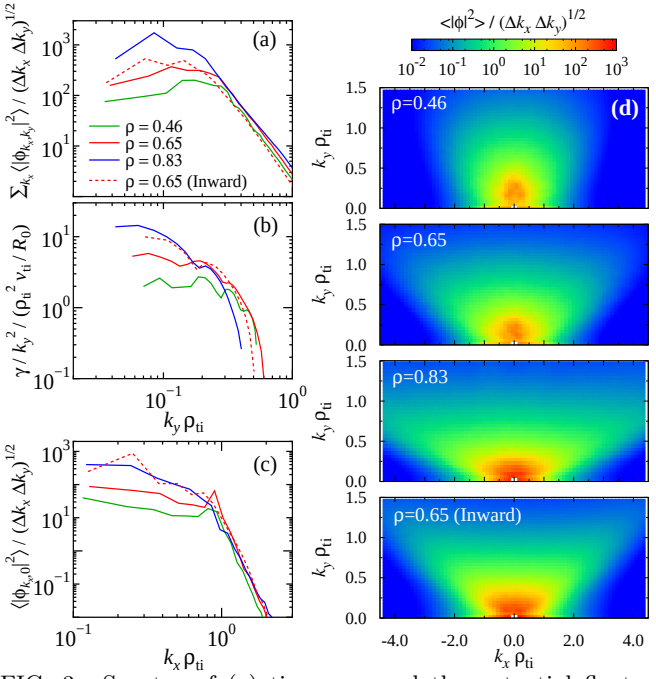

FIG. 3. Spectra of (a) time-averaged the potential fluctuations in k_y space integrated over k_x space, (b) linear ITG growth rates divided by square of the wavenumber k_y, (c) time-averaged zonal flow potentials in k_x space, and (d) time-averaged potential fluctuations in (k_x, k_y) space at $\rho = 0.46$, 0.65 and 0.83 in the experimental case, and at $\rho = 0.65$ in the inward-shifted case. In (a), (c) and (d), ϕ and $(\Delta k_x,\ \Delta k_y)$ are normalized by $eR_0/T_i\rho_{ti}$ and ρ_{ti}, respectively.

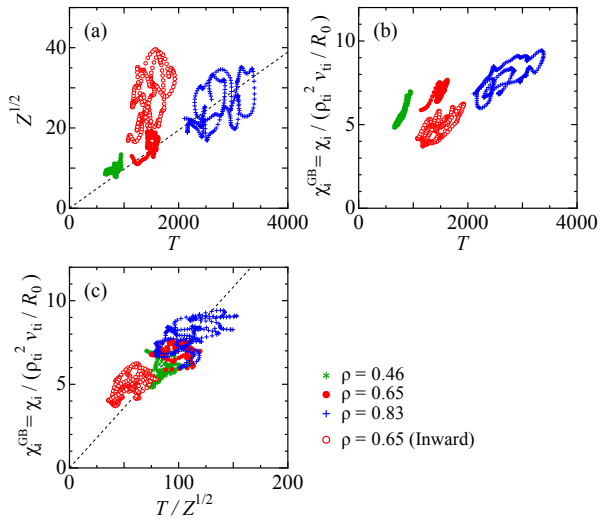

FIG. 4. Lissajous plots of the ITG turbulence simulations of the saturated phases in (a) $(T, Z^{1/2})$-space, in (b) (T, χ_i^{GB})-space, and in (c) $(T/Z^{1/2}, \chi_i^{GB})$-space for the experimental cases at $\rho = 0.46, 0.65$ and 0.83, and the inward-shifted LHD case at $\rho = 0.65$, where χ_i^{GB} is the ion heat diffusivity in gyro-Bohm unit defined as $\chi_i^{GB} \equiv \chi_i/(\rho_{ti}^2 v_{ti}/R_0)$. Dashed lines in (a) and (c) represent $Z^{1/2} = \lambda T$ with $\lambda = 9.7 \times 10^{-3}$ and $\chi_i^{GB} = \kappa T/Z^{1/2}$ with $\kappa = 7.2 \times 10^{-2}$, respectively. Here, $T \equiv (1/2)\sum_{k_x,k_y\neq 0}\langle|\phi_{k_x,k_y}|^2\rangle/(\Delta k_x \Delta k_y)^{1/2}$ and $Z \equiv (1/2)\sum_{k_x}\langle|\phi_{k_x,0}|^2\rangle/(\Delta k_x \Delta k_y)^{1/2}$, where ϕ and $(\Delta k_x,\ \Delta k_y)$ are normalized by $eR_0/T_i\rho_{ti}$ and ρ_{ti}, respectively.

the LHD experiments and future helical reactors based on the gyrokinetic simulations. The present simulations also verify that zonal flows, which are more efficiently generated by the neoclassical optimized configuration, induce the spectral transfer of the potential fluctuation into the less-unstable high-k_x region and consequently cause the regulation of turbulent transport. The simple relation obtained from the simulations, which describes the strong correlation between the turbulent heat diffusivity and the ratio of the turbulence fluctuation energy to the zonal flow amplitude, is expected to contribute to the anomalous transport modeling for helical plasmas.

The authors would like to thank the LHD experiment group for providing data and fruitful discussions. This work is supported in part by the Japanese Ministry of Education, Culture, Sports, Science and Technology, Grant No. 22760660, and 21560861, and in part by the NIFS Collaborative Research Program, NIFS11KNST017, NIFS11KNXN229, NIFS10KNTT003, and NIFS10KNST006.

[1] M. Wakatani, *Stellarator and Heliotron Devices* (Oxford University Press, 1998).
[2] S. Murakami *et al.*, Nucl. Fusion **42**, L19 (2002).
[3] T.-H. Watanabe, H. Sugama and S. Ferrando-Margalet, Phys. Rev. Lett. **100**, 195002 (2008).
[4] H. E. Mynick, N. Pomphrey and P. Xanthopoulos, Phys. Rev. Lett. **105**, 095004 (2010).
[5] P. H. Diamond, S.-I. Itoh and K. Itoh, *Modern Plasma Physics: Volume 1* (Cambridge University Press, 2010).
[6] P. H. Diamond *et al.*, Plasma Phys. Control. Fusion **47**, R35 (2005).
[7] C. Hidalgo, Plasma Phys. Control. Fusion **53**, 074003 (2011).
[8] A. M. Dimits *et al.*, Phys. Plasmas **7**, 969 (2000).
[9] X. Garbet *et al.*, Nucl. Fusion **50** 043002 (2010).
[10] T.-H. Watanabe, H. Sugama and S. Ferrando-Margalet, Nucl. Fusion **47**, 1383 (2007).
[11] P. Xanthopoulos, F. Merz, T. Görler and F. Jenko, Phys. Rev. Lett. **99**, 035002 (2007).
[12] T. L. Rhodes *et al.*, Nucl. Fusion **51**, 063022 (2011).
[13] A. Komori *et al.*, Fusion Sci. Technol. **58**, 1 (2010).
[14] M. Nunami *et al.*, Plasma Fusion Res. **6**, 1403001 (2011).
[15] K. Tanaka *et al.*, Rev. Sci. Instrum. **79**, 10E702 (2008).
[16] K. Tanaka *et al.*, Plasma Fusion Res. **5**, S2053 (2010).
[17] M. Nunami *et al.*, Plasma Fusion Res. **5**, 016 (2010).
[18] S. P. Hirshman and O. Betancourt, J. Comput. Phys. **96**, 99 (1991).
[19] M. A. Beer, S. C. Cowley and G. W. Hammett, Phys. Plasmas **2**, 2687 (1995).
[20] A. H. Boozer, Phys. Fluids **11**, 904 (1980).
[21] C. D. Beidler and H Maaßberg, Plasma Phys. Control. Fusion **43**, 1131 (2001).
[22] H. Sugama and T.-H. Watanabe, Phys. Plasmas **13**, 012501 (2006).
[23] P. Helander *et al.*, Plasma Phys. Control. Fusion **53**, 054006 (2011).
[24] H. E. Mynick and A. H. Boozer, Phys. Plasmas **14**, 072507 (2007).
[25] J. Wesson, *Tokamaks Second Edition* (Oxford University Press, 1997), p. 198.
[26] M. Nakata, T.-H. Watanabe and H. Sugama, (submitted).